Published version available at: https://doi.org/10.1016/j.combustflame.2023.112988

# Multiplicity of solutions of lifted jet edge flames: symmetrical and non-symmetrical configurations

Carmen Jiménez, Vadim N. Kurdyumov*

*Department of Energy, CIEMAT, Avda. Complutense 22, 28040 Madrid, Spain*

**Abstract**

A numerical investigation of the combustion process taking place after fuel and oxidizer are injected separately into a planar channel from an end-wall porous plug is presented. A fuel stream injected in the middle of the channel is surrounded on both sides by oxidizer streams and two edge flames are formed after contact of reactants and ignition. The formulation of the problem is symmetrical with respect to the middle of the channel. The study is based on the coupled Navier-Stokes and transport equations with one-step Arrhenius-type combustion kinetics. The main focus is on the influence of the fuel Lewis number, the flow rate and the Damköhler number on the flame structure.

It is shown that symmetrical and non-symmetrical configurations of edge flames are possible for the same set of parameters, and that these solutions can be simultaneously stable. At the same time, the areas of existence of symmetric and non-symmetric flame configurations turn out to be different. Further, it is demonstrated that there can be at least seven different (but not all stable) steady-state solutions for the same set of parameters, although the evidence for the absence of other solutions, in addition to those found, cannot be achieved within the framework of the methods used in the study. These results may be critical for flames with low fuel Lewis number (e.g. hydrogen flames) and highlight the importance of taking into account the possibility of non-symmetrical flame configurations in the design and operation of combustion devices based on diffusion flames.

*Key words:* edge flame, diffusion flame, non-symmetric flames, mixing

*Fax: +34 91 346 6269.

*Email address:* vadim.k@ciemat.es (Vadim N. Kurdyumov)

layer

---

## Novelty and significance statement

In this work, the appearance of non-symmetric structures for diffusion combustion is investigated for the first time within the framework of the coupled Navier-Stokes and transport equations. In the considered configuration fuel and oxidizer are injected from a porous plug into a planar channel forming two edge flames. The simultaneous appearance of symmetrically and non-symmetrically situated edge flames is demonstrated, and the regions of existence of such structures are investigated.

## Authors contributions

CJ - performed research, wrote the paper; VNK - performed research, wrote the paper.

## 1. Introduction

It is known that one of the most reliable configurations for injecting fuel and oxidizer into a combustion chamber is to inject them through different ducts without premixing. This avoids such dangerous situations as the flashback effect, when the flame can propagate upstream into the injection conduct if the fuel and oxidizer are readily mixed before injection.

In a recent study [1] carried out within the constant density model, it was shown that the separate fuel and oxidizer injection in the form of parallel streams in a perfectly symmetric set-up can lead to a solution featuring flames located non-symmetrically about the axis, in addition to a symmetrical solution, which can also exist. These two solutions, symmetrical and not symmetrical, differ significantly from each other in their properties, regions of existence, etc. Although the thermal-diffusive or constant-density model has proven to be reliable for studying many phenomena from a qualitative point of view, some important aspects of the combustion process, such as the effect of thermal expansion, remain without due attention within that framework. The present study aims at filling this gap and incorporates the effects of combustion heat release on the density, the flow and the resulting flames.

Historically, attention to what is now called the edge flame [1] did not begin until the penultimate decade of the last century. One of the reasons for this attention was the understanding of the importance of this structure in turbulent combustion [2]. Investigations on edge flames can be classified into two large groups. The first group of studies focuses on moving edge flames and propagation speed itself is to be found as part of the solution, see [3, 4, 5, 6, 7, 8, 9, 10, 11, 12, 13]. Another group of investigations is mainly concerned with the structure and dynamics of the edge flame located near the tip of the splitter plate separating fuel and oxidizer streams [14, 15, 16, 17, 18, 19, 20, 21, 22]. Other configurations have also been investigated, for example in the corner region of two mutually perpendicular streams of fuel and oxidizer, see [23]. Important references to other earlier works can be found in [24, 25], and a general overview of experimental results in [26]. A recent review of issues related to diffusion flames involving edge flames with a focus on the effect of hydrodynamics is presented in [27].

Many of the aforementioned studies adopted the constant density approximation, which conveniently separates hydrodynamics from the heat and mass transport equations. The only exceptions are the studies presented in [17, 18, 22], in which thermal expansion was taken into account. It is important to note that in all the above studies, only a single edge flame was considered. The effect of the interaction of two closely spaced flame edges leading to the breaking of symmetry for this type of diffusion flames was not investigated systematically (with the exception of [1], to the best of the authors' knowledge), although some researchers seem to have encountered this effect in numerical simulations, see Ph. D thesis by J. Carpio [28]. Interestingly, on page 109 of [28] , there is a picture of a non-axisymmetric diffusion flame in a round jet, obtained at IRPHE years ago by P. Martínez-Legapzi and J.M. Truffaut, unpublished to our knowledge.

The phenomenon of symmetry breaking has received due attention recently for premixed combustion. Symmetry breaking occurs, for example, when a premixed flame propagates freely in a channel. It has been shown that symmetric and non-symmetric flames (with respect to the channel axis in circular channels or the mid-plane in planar channels) may appear in this case, see e.g. [29, 30, 31, 32, 33, 34]. This effect is associated with the strong

[1] Other names are "triple flame" and "tribrachial flame". However, the name "edge flame" seems to have become more stable in modern literature.

nonlinearity of the governing equations and the fact that the non-symmetric configuration can be more stable than the symmetric one for the same set of parameters.

Solving the coupled Navier-Stokes and transport equations with detailed chemistry including a wide range of variation of the parameters is a formidable task. The use of simplified chemical kinetics, even if neglecting some details, reduces the number of parameters involved and enables a more complete description of the problem with deeper physical understanding. The model adopted in the present study assumes an overall one-step chemical reaction scheme and constant gas properties. These simplifications will be relaxed in future studies. However, as can be seen below, comparing these results with those presented in [1], where a simpler model was used, one can conclude that the effects obtained and their parametric trends appear to be qualitatively (and to some extent quantitatively) similar, indicating structural robustness of the phenomena under consideration.

The article is organized as follows: Section 2 presents the problem statement. Section 3 briefly describes the methods used to obtain numerical solutions. Section 4 presents the results obtained, while the last section suggests the conclusions drawn by the authors.

## 2. Formulation

Streams of fuel and oxidizer are injected separately through a porous plug situated at the end-wall of a planar semi-infinite channel of width $2H$, as shown in Fig. 1 where the situation without combustion is sketched. The fuel is injected along a section of the plug of length $L$ located in the center of the channel, and the oxidizer is injected from the rest of the porous surface. It is assumed that the fuel and oxidizer do not mix inside the porous layer. The gas streams emerge from the porous surface with the same uniform normal velocity $U$. It is important to note that the injection configuration of reactants considered in the present study is absolutely symmetrical with respect to the $y = 0$ axis.

The thermal conductivity of the plug volume is assumed sufficiently high so as to maintain the gas temperature at the porous plug exit uniform and equal to $T_0$. The channel walls are impermeable and maintained at the same temperature, $T_0$. At the exit of the plug the reactants mass fraction fluxes are specified. Two mixing layers are produced downstream the porous surface in which the fuel and oxidizer interdiffuse.

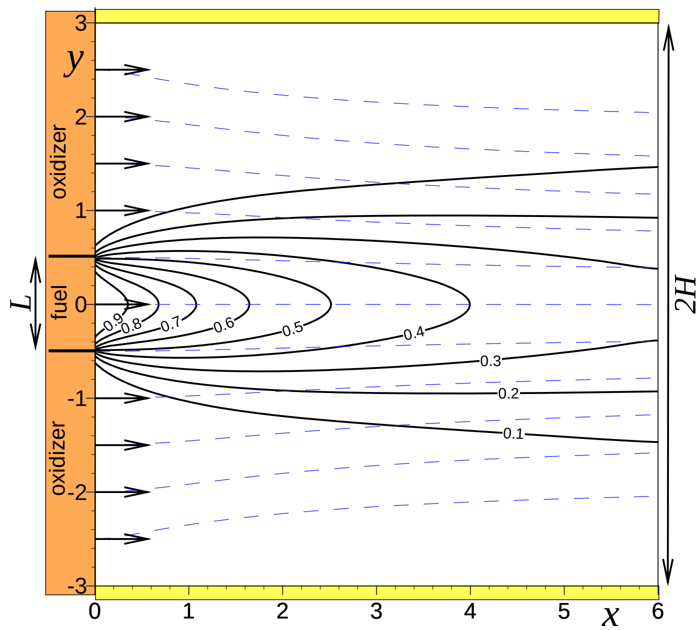


Figure 1: Sketch of the problem, coordinate system, distributions of the normalized mass fraction of fuel (solid isolines, with an interval of 0.1) and the stream function (dashed isolines, with an interval of 5) plotted for $m = 10$ and the frozen case, $D = 0$.

The chemical reaction between the fuel and oxidizer is modeled by an overall irreversible one step reaction of the form

$$\text{Fuel} + \nu\,\text{Oxidizer} \rightarrow (1+\nu)\text{Product},$$

where $\nu$ is the mass-weighted stoichiometric coefficient. The fuel consumption rate per unit volume is assumed to be first order with respect to each of the two reactants and to obey a standard Arrhenius law, $\Omega = \mathcal{B}\rho^2 Y_F Y_O \exp(-\mathcal{E}/\mathcal{R}T)$, with a preexponential factor $\mathcal{B}$ and an overall activation energy $\mathcal{E}$. Here $Y_F$ and $Y_O$ are the mass fractions of fuel and oxidizer, respectively, $T$ and $\rho$ are the temperature and density of the mixture, and $\mathcal{R}$ is the universal gas constant.

The heating effect due to viscous dissipation is neglected due to its insignificance compared to the heat released by combustion. Assuming a low-

Mach number approximation, the standard (dimensionless) governing equations become

$$\partial\rho/\partial t + \nabla\cdot\rho\mathbf{v} = 0, \tag{1}$$

$$\rho\,\partial\theta/\partial t + \rho\mathbf{v}\cdot\nabla\theta = \nabla^2\theta + (1+\phi)\omega, \tag{2}$$

$$\rho\,\partial Y_F/\partial t + \rho\mathbf{v}\cdot\nabla Y_F = Le_F^{-1}\nabla^2 Y_F - \omega, \tag{3}$$

$$\rho\,\partial Y_O/\partial t + \rho\mathbf{v}\cdot\nabla Y_O = Le_O^{-1}\nabla^2 Y_O - \phi\,\omega, \tag{4}$$

$$\rho\,\partial\mathbf{v}/\partial t + (\rho\mathbf{v}\cdot\nabla)\mathbf{v} = -\nabla p + Pr(\nabla^2\mathbf{v} + \nabla(\nabla\cdot\mathbf{v})/3)\,, \tag{5}$$

$$\rho\,(1+q\theta) = 1\,, \tag{6}$$

where $\mathbf{v} = u\mathbf{e}_x + v\mathbf{e}_y$ is the velocity vector with $u$, $v$ the corresponding velocity components.

In writing these equations the initial width of the fuel stream, $L$, was chosen as a unit of length, the characteristic velocity $\mathcal{D}_T/L$ as a unit of speed and $L^2/\mathcal{D}_T$ as a unit of time; here $\mathcal{D}_T$ is the thermal diffusivity of the mixture. The mixture density $\rho$ and the mass fractions $Y_F, Y_O$ were normalized with respect to their values in the supply streams, $\rho_0$ and $Y_{F_0}, Y_{O_0}$, and a non-dimensional temperature $\theta = (T-T_0)/(T_a-T_0)$ was introduced, where $T_a = T_0 + QY_{F_0}/[c_p(1+\phi)]$ is the adiabatic temperature with $Q$ the heat release rate (per unit mass of fuel), $\phi = \nu Y_{F_0}/Y_{O_0}$ is the initial mixture equivalence ratio and $c_p$ is the specific heat.

The boundary conditions at the porous plug surface, $x=0$, are

$$\begin{aligned} &\rho = 1, \quad \theta = 0, \quad u = m, \quad v = 0\,, \\ &mY_F - \frac{1}{Le_F}\frac{\partial Y_F}{\partial x} = \begin{cases} m, & |y| < 1/2 \\ 0, & |y| > 1/2 \end{cases}, \\ &mY_O - \tfrac{1}{Le_O}\tfrac{\partial Y_O}{\partial x} = \begin{cases} 0, & |y| < 1/2 \\ m, & |y| > 1/2 \end{cases}. \end{aligned} \tag{7}$$

Here we assume that injection occurs in the direction normal to the porous surface. Downstream we impose

$$x\to\infty: \quad \partial^2\theta/\partial x^2 = \partial^2 Y_F/\partial x^2 = \partial^2 Y_O/\partial x^2 = \partial u/\partial x = v = 0\,, \tag{8}$$

where zero second derivatives in $x$ direction are imposed for the temperature and mass fractions. These conditions are weaker than the zero temperature requirement that must be required further downstream due to sidewall cooling.

The channel walls are isothermal, impermeable for fuel and oxidizer with non-slip conditions for the gas velocity

$$y = \pm h: \quad \theta = 0, \quad \partial Y_F/\partial y = \partial Y_O/\partial y = 0, \quad u = v = 0\,. \tag{9}$$

Anticipating the results presented below, some calculations will also be carried out in a half-width domain. In these cases, the standard symmetry boundary conditions are set,

$$y = 0: \quad \partial\theta/\partial y = \partial Y_F/\partial y = \partial Y_O/\partial y = \partial u/\partial y = v = 0. \tag{10}$$

The dimensionless parameters in Eqs. (1)-(7) are the Prandtl number $Pr = c_p\mu/\lambda$, where $\mu$ and $\lambda$ are the viscosity and thermal conductivity, the injection gas velocity $m = UL/\mathcal{D}_T$, the channel half-width $h = H/L$, the Lewis numbers associated with the fuel and oxidizer $Le_F = \mathcal{D}_T/\mathcal{D}_F$ and $Le_O = \mathcal{D}_T/\mathcal{D}_O$, where $\mathcal{D}_F$ and $\mathcal{D}_O$ are the molecular diffusivities of the fuel and oxidizer, respectively, and the thermal expansion parameter $q = (T_a - T_0)/T_0$.

Assuming a global one-step chemical reaction, the dimensionless reaction rate is given by

$$\omega = D\beta^3\rho^2 Y_F Y_O \exp\left[\frac{\beta(\theta-1)}{(1+q\theta)/(1+q)}\right], \tag{11}$$

where $\beta = \mathcal{E}(T_a - T_0)/\mathcal{R}T_a^2$ and $D = (L^2/\mathcal{D}_T)\cdot\mathcal{B}\rho_0 Y_{O_0}\beta^{-3}\exp\left[-\mathcal{E}/\mathcal{R}T_a\right]$ are the Zel'dovich and Damköhler numbers, respectively. Historically, the factor $\beta^3$ is introduced into the definition of the Damköhler number for convenience, as done for example in [14, 15, 16]. This is related to the asymptotic calculation of the planar flame speed along the stoichiometric surface.

In the present work, both steady-state and time-dependent solutions are investigated. To simulate the dynamical regimes numerically, cold distributions of all variables perturbed by the addition of a hot spot of the form

$$\delta\theta = A\exp(-[(x-x_*)^2 + (y-y_*)^2]/r_0^2] \tag{12}$$

with $r_0 = 0.5$ were used as initial conditions. Specific values $x_*$ and $y_*$ for the hot spot location will be presented below. In the case of an iterative procedure for finding steady-state solutions, similar initial conditions were chosen, which, however, are not relevant.

When setting dimensionless parameters for the combustion process, the dimensionless activation energy, $N = \mathcal{E}/\mathcal{R}T_0$, is often used instead of the Zel'dovich number. Because $\beta = Nq/(1+q)^2$, an increase in the Zel'dovich number occurs with a decrease in $q$ (at a fixed activation energy $\mathcal{E}$), that is, for leaner mixtures. Due to the significant number of parameters appearing in the problem, we fix the values $q = 5$ and $Pr = 0.72$, which are typical values for combustible mixtures. Also, for all the results presented below we use $Le_O = 1$, $\phi = 1$ and $h = 3$. Although most of the results are obtained for $\beta = 10$, which corresponds to the value of the dimensionless activation energy $N = 72$, the influence of the Zel'dovich number is also considered.

In order to characterize the flame structure quantitatively, a symmetry index was calculated in the form

$$S = \int\limits_0^\infty dx \int\limits_0^h [\theta(x,y,t) - \theta(x,-y,t)]dy\,. \tag{13}$$

For the two-dimensional planar case considered in the paper, this value represents a convenient magnitude for identifying the symmetry of solutions with respect to the $y = 0$ axis[2]. Clearly, $S = 0$ (within numerical accuracy) for symmetric solutions, but it takes a nonzero value when the solution becomes non-symmetric. Perhaps one can imagine a distribution that is non-symmetric with respect to $y = 0$ and at the same time has a zero value for $S$. However, one can be sure that if $S \neq 0$ the distribution is indeed non-symmetric. It should also be noted that the equations are solved in domains of finite $x$ length, therefore the values for $S \gtreqless 0$ should be compared only in domains of the same size.

To determine the edge flame position, we will use point $(x_w, y_w)$ at which the reaction rate $\omega$ reaches a local maximum value, $\omega_{max} = \omega(x_w, y_w)$. In the considered configuration there are two edge flames located at $(x_{w1}, y_{w1})$ with $y_{w1} < 0$ (the lower half-plane) and $(x_{w2}, y_{w2})$ with $y_{w2} > 0$ (the upper half-plane). Obviously, for a symmetrical flame structure we have $x_{w1} = x_{w2}$ and $y_{w1} = -y_{w2}$. Anticipating the results presented below, in some cases the two edge flames merge into one located on the axis of symmetry and $x_{w1} = x_{w2}$ together with $y_{w1} \approx y_{w2} \approx 0$ was observed. For the results presented below, we will determine the positions of the edge flames always with $x_{w1} \leqslant x_{w2}$.

[2] Of course, one can determine the symmetry index in another way. For example, the additional factor $y$ for the sub-integral expression was included in its definition in [1].

Additionally, two points should be noted. Firstly, it is clear that for each non-symmetric solution reported below there exists a mirror one reflected with respect to the line of symmetry $y = 0$. This circumstance will no longer be noted specifically in the following. Secondly, symmetric solutions can be obtained using half-domain simulations, which was done in some cases. It was verified that the symmetric solutions calculated in the half-width domain match those in the full domain in all the corresponding cases, as it should be.

## 3. Numerical treatment

Steady as well as time-dependent solutions of Eqs. (1)-(6) are reported below. All calculations were carried out for $0 < x < x_{max}$. For the considered ranges of parameters, the typical values for $x_{max}$ were between 6 and 10. It was verified that changing the domain size within these values does not affect the characteristics of the solutions obtained.

The main goal of the study is to demonstrate that despite the symmetrical configuration of the problem (the governing equations and boundary conditions are symmetric about the axis $y = 0$), in addition to the expected symmetric solutions, there are non-symmetric solutions for some parameter values. For this reason, calculations were made both in the full domain, $-h < y < h$, and in a half-width domain, $-h < y < 0$, using the boundary conditions Eq. (10).

To confirm and verify the results of the present study, several types of numerical procedures were applied. It is advantageous for numerical simulations to eliminate the pressure from the momentum equation by introducing the vorticity field, $\zeta = v_x - u_y$, where subscripts, here and below, denote partial differentiation. Taking the curl of Eq. (5) one finds that $\zeta$ satisfies

$$\rho\zeta_t + \rho\mathbf{v}\cdot\zeta = Pr\nabla^2\zeta + J, \tag{14}$$

where $J$ is the vorticity production term given by

$$J = (\rho_y u_t - \rho_x v_t) + [(\rho u)_y u_x - (\rho u)_x v_x] + [(\rho v)_y u_y - (\rho v)_x v_y]\,.$$

To obtain the steady-state solutions (perhaps unstable in some cases), the counterpart of Eqs. (2)-(4) and (14) by setting $\partial/\partial t \equiv 0$ is considered. The continuity equation is satisfied automatically by introducing a stream function $\psi$, defined from $\rho u = \psi_y$, $\rho v = -\psi_x$, which satisfies

$$(\psi_x/\rho)_x + (\psi_y/\rho)_y = -\zeta\,. \tag{15}$$

The elliptic system (2)-(4) and (14)-(15) for $\zeta$ and $\psi$ and the remaining state variables was solved using a Gauss-Seidel iteration method with successive overrelaxation.

All the steady-state solutions reported below were obtained using second-order, three-points central differences for spatial derivatives on a rectangular uniform grid with equal steps in both directions. The numerical grid size was varied as 1/40, 1/60 and 1/80. Anticipating the results of the calculations, the positions of the edge flame closest to the porous plug were obtained equal to $x_{w1} = 0.4735$, 0.4692, and 0.4678, in grids with sizes 1/40, 1/60 and 1/80, respectively, in calculations with $x_{max} = 6$, $m = 10$, $N = 72$, $Le_F = 0.7$ and $D = 1500$. When calculating with $x_{max} = 10$ on a grid with size 1/40, the position of the flame was $x_{w1} = 0.4734$. It can be concluded that although there are slight changes (of less than 1.5%) in the position of the edge flame, this cannot affect the main results of the calculations.

Two Gauss-Seidel iteration procedures were applied to calculate steady-state solutions. In the first case, direct iterative calculations of all distributions were performed with fixed values for all parameters. In the second case, the temperature value, $\theta = \theta_*$, was fixed at one point of the domain while the value of the Damköhler number $D$ was calculated iteratively also by the Gauss-Seidel method with relaxation. The choice of the temperature $\theta_*$ and its location had to correspond to some real solution (stable or unstable). To ensure this, a previously calculated solution was shifted by several grid points downstream/upstream and used as the initial condition for iterations. The typical values for $\theta_*$ were between 0.7 and 0.8 fixed in a point along the $y = \pm 1/2$ line.

To calculate time dependent solutions, a compressible Navier-Stokes solver described in [35] with 6th-order finite differences and 3d order Runge-Kutta time-integration was used. The typical Mach number for these calculations was of order $10^{-3}$. These calculations using a compressible code were done for two reasons. On the one hand, the numerical method of [35] is well tested by many researchers, although it does not allow finding unstable solutions. On the other hand, the authors wanted to verify the results by two very different methods. Looking ahead, one can say that this has been achieved.

All time dependent calculations were carried out in the full domain. It should be noted that the study of the ignition process was not the goal of the present investigation. For this reason, the minimum value of the applied energy required for ignition has not been investigated. Time dependent calculations were carried out only to verify the stability of the steady-state solutions obtained using the Gauss-Seidel method.

## 4. Results

The numerical modeling of symmetric and non-symmetric structures presented in [1] was done on the basis of time-dependent calculations and within the framework of the constant density model. Such an approach automatically provides knowledge of the stability of one or another state. However, it leaves open the question of possible additional steady-state but unstable solutions, since it is obvious that only stable states can be found in this way. The method of iterative calculation of steady states is partially devoid of this shortcoming, since some of the unstable states can also be found.

The problem of finding all of the steady-state solutions for the coupled Navier-Stokes and transport equations is a formidable task, even within a two-dimensional model. The results presented below demonstrate the multiplicity of steady-state solutions for some parameter values or ranges of values. However, the authors do not intend to provide a rigorous mathematical proof that all possible steady-state solutions have been obtained. This task lies aside from the main goal of this study.

### *4.1. Steady-state solutions*

Fig. 2 illustrates two different steady-state solutions calculated with the same set of parameters, $m = 10$, $D = 1500$, $N = 72$ and $Le_F = 0.7$. The colored shadings show the temperature field, the black lines correspond to reaction rate isolevels and the white lines represent the streamlines. It can be seen in the left plot that the locations of the two edge flames are non-symmetrical about the $y = 0$ axis, namely, the edge flame located in the lower half-plane is closer to the porous plug than the upper one. In the right plot, the two edge flames are located at an equal distance from the porous plug and symmetrically with respect to the $y = 0$ axis.

A direct linear stability analysis of solutions is not performed in the present paper. However, anticipating the results of time-dependent calculations, both solutions, symmetric and non-symmetric, are apparently stable. The existence of these two kinds of solutions was reported in [1] within the framework of the constant density model. In [1] it was also shown also by time dependent calculations that the symmetric and non-symmetric configurations were both stable, that is, the actual occurrence of one or the other structure depends on the initial conditions.

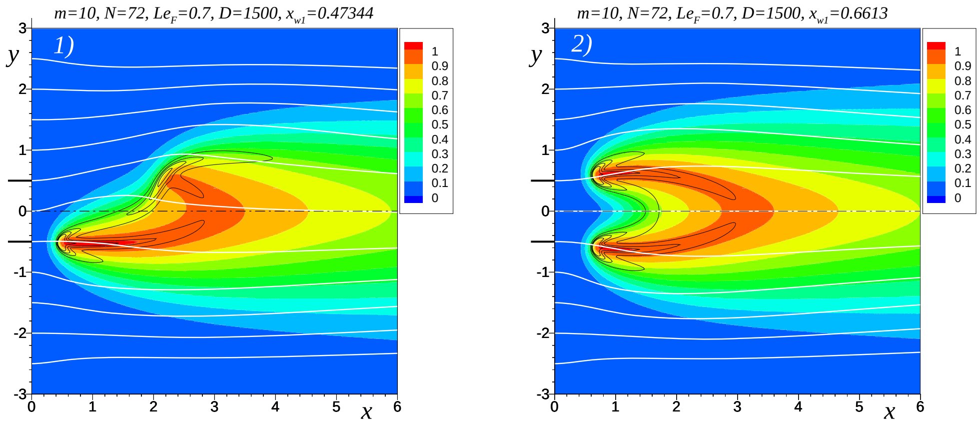


Figure 2: Example of two flame structures, non-symmetrical (left plot) and symmetrical (right plot) calculated with the same set of parameters, $m = 10$, $D = 1500$, $N = 72$ and $Le_F = 0.7$. The solutions correspond to points 1) and 2) in Fig. 6; the color shades show the temperature field, black and white lines show $\omega$-isolines ($\omega = 1$, 5, 10 and 20) and $\psi$-isolines (with an interval of 5), respectively.

The observed differences in the two flame structures affect the interaction between the flames and the porous plug. Figure 3 illustrates this by comparing the heat fluxes into the porous plug for the symmetrical and non-symmetrical cases shown in the previous figure. Since the dimensionless temperature of the porous plug is zero, the heat flux into the porous plug is determined only by $q = \partial\theta/\partial x|_{x=0}$, despite the nonzero value of the gas velocity on it. It can be seen that for the non-symmetric case, the maximum value of the heat flux into the porous plug is significantly higher than for the symmetric configuration.

Shown in Fig. 4 are the dependencies on the Zeldovich number of the symmetry index $S$ (solid line) and the positions of the leading edge flame $x_{w1}$ for the symmetrical (dashed line) and non-symmetrical (dash-dotted line) solutions, calculated for $m = 10$, $D = 1500$ and $Le_F = 0.7$. It can be seen that the change in the Zel'dovich number has a relatively modest quantitative effect.

Numerical analysis shows that the dependence of the positions of the edge flame on the Damköhler number has a complex multi-valued character.

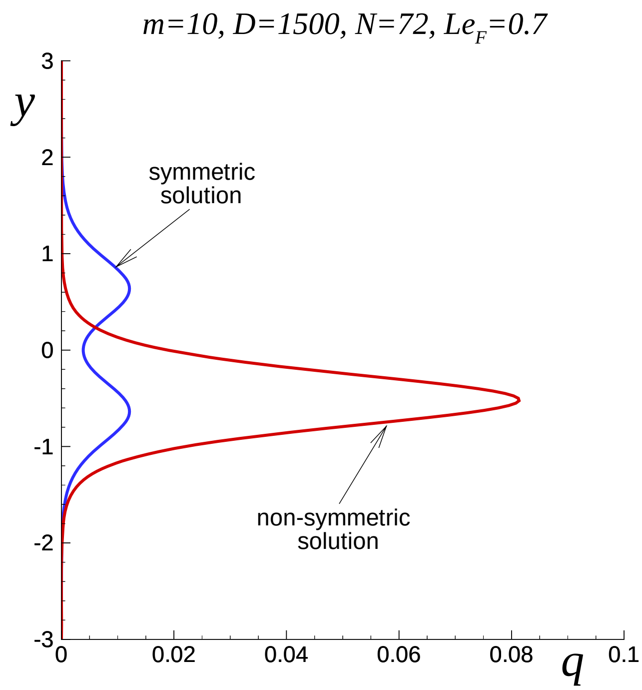


Figure 3: Dependence of the heat flux $q$ on $y$ along the porous plug for symmetrical and non-symmetrical configurations, for $m = 10$, $D = 1500$, $N = 72$ and $Le_F = 0.7$.

Figure 5 illustrates the dependence of the distance from the edge flame to the porous plug on the Damköhler number calculated for $m = 10$, $N = 72$ (or $\beta = 10$) and $Le_F = 0.7$. The curves drawn with solid and dashed lines represent $x_{w1}$ and $x_{w2}$ for the positions of the forward and behind edge flames, respectively, for the non-symmetric solutions. The dashed-dotted curve represents the position of the flames in the symmetric configuration where $x_{w1} = x_{w2} = x_w$. It can be seen that there is an interval of $D$ within which symmetric and non-symmetric solutions exist simultaneously, which has already been illustrated in Fig. 2. The branch of non-symmetric solutions has a typical C-shape, that is, there are two non-symmetric solutions for a given Damköhler number. Interestingly, the branch of symmetric solutions has a double C-shape, that is, there can be up to four different symmetric steady-state solutions (probably, not all of them stable).

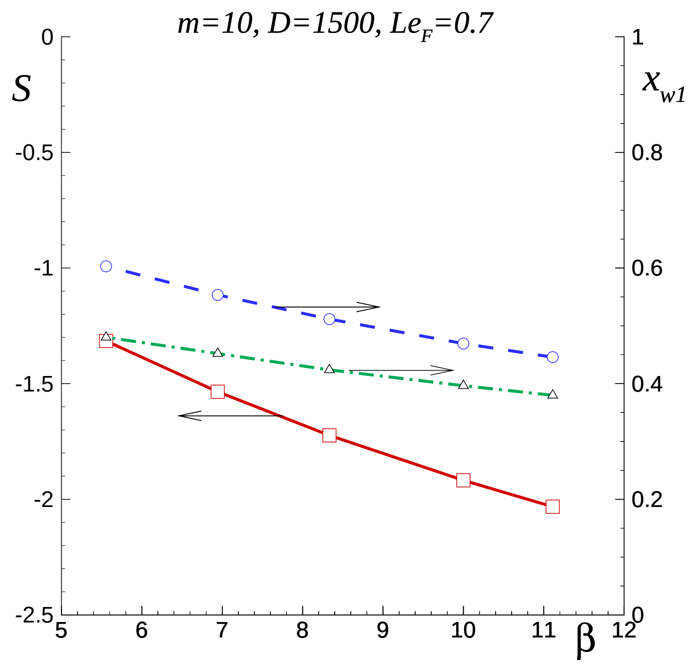


Figure 4: The symmetry index $S$ (solid line) and the position of the leading edge flame for the symmetrical (dashed line) and non-symmetrical (dash-dotted line) cases versus the Zel'dovich number, for $m = 10$, $D = 1500$ and $Le_F = 0.7$.

The curves in Fig. 5 show that there are two qualitatively different types of dependencies of the edge flame positions on the Damköhler number. In the first case, as $D$ increases, the value of $x_{w1}$ decreases. However, there are segments that are qualitatively different from this behavior, for which $x_{w1}$ increases with $D$. Although the linear analysis of stability is left out of this work, it is natural to assume that only for the first type of dependencies ($x_{w1}$ decreases with increasing $D$), the flame configuration can be stable while for other "anomalous" segments the steady-states are not stable.

Obviously, the lower branch of the dashed-dotted curve (symmetric solutions) can be extended to arbitrarily large Damköhler numbers. The edge flame position $x_w$ gradually approaches the porous plug when $D \to \infty$. However, numerical analysis showed that at $D \to \infty$ there is another branch of

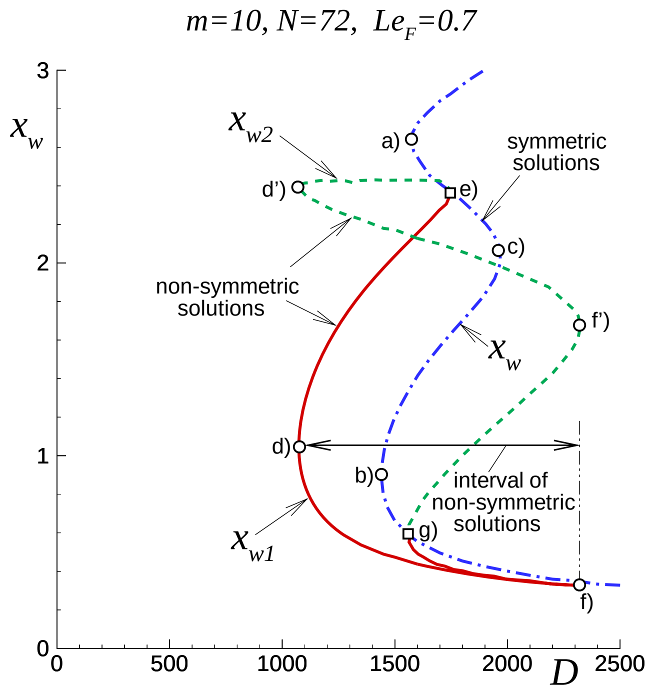


Figure 5: Dependence of the edge flame position on the Damköhler number for $m = 10$, $N = 72$ and $Le_F = 0.7$. The solid and dashed lines show $x_{w1}$ and $x_{w2}$, respectively, for non-symmetrical flames, the dash-dotted line represents $x_w$ for symmetrical flames; open circles mark the turning points; open squares indicate the bifurcation points.

solutions for which $x_w$ increases with $D$. It should be noted that as we move along this branch, the calculations become more and more stiff. The continuation of this branch would resemble the unstable branch appearing in the problem of a premixed flame in a channel with heat losses, see[36]. Indeed, the position of the flame away from the porous wall leads to an almost premixed state of the reactants in front of the flame, since they have time to partially mix during the convection from the porous plug to the flame.

Fig. 5 shows that the solid curve (position $x_{w1}$) and the dashed curve (position $x_{w2}$) for the branch of non-symmetric solutions have bifurcation points connecting this curve with the branch of symmetric solutions (dash-dotted line). These points are marked with open squares and the letters e) and g). These solid and dashed curves also have turning points marked with open circles and the letters d), f) on the solid line and d′), f′) on the dashed line.

Perhaps Fig. 5 requires more detailed explanations. The segment of the solid curve (for $x_{w1}$) between points g) and f) corresponds to the part of the dashed curve (for $x_{w2}$) between points g) and f′), the segment of the solid curve between points f) and d) corresponds to the part of the dashed curve between f′) and d′), and, finally, the segment of the solid curve between d) and e) corresponds to the part of the dashed curve between d′) and e). The interval of Damköhler numbers between points d) and f) corresponds to the region of existence of non-symmetrical flame configurations. We also note that the parts of the solid response curve corresponding to $x_{w1}$, namely the part going to the right to the turning point f) with increasing $D$ and the part returning to the left from the turning point, merge practically into one curve in the vicinity of the point f) and are separated from each other only near the bifurcation point g).

It is interesting to find that the dashed-dotted curve corresponding to symmetric solutions has three turning points, namely a), b) and c). Since for the segment between points a) and c) the value of $x_w$ decreases with increasing $D$, it can be assumed that the (symmetrical) flame states corresponding to at least a part of this segment are also stable, in addition to the segment of the dashed-dotted curve going from point b) to the right. Anticipating the results presented in Section 4.2, this assumption will be confirmed by time-dependent calculations.

Fig. 5 shows that the dependence of the edge flame position on the Damköhler number is complex and multiple-valued. In order to represent more clearly the multiplicity of modes, the response curves for $x_{w1}$ and $x_w$ are drawn in Fig. 6 in more detail. For the parameter values marked with filled triangles in this figure, the distributions of temperature, reaction rate, and stream function are presented in Figs. 2 (solutions 1 and 2) and 7 (solutions 3, 4, 5, 6 and 7). One can see in Fig. 7 for solutions 5) and 6) that when the flame moves away from the porous plug, the two initially separated flame edges merge into one located on the channel axis.

Although the distributions shown in Fig. 7 were not obtained for the same Damköhler number (this was done to separate the points given by triangles in Fig. 6), it is obvious that for some values of $D$ (for example, $D \approx 1600$) there are at least seven different steady flame configurations. Anticipating the time-dependent results presented in section 4.2, one can conclude that at

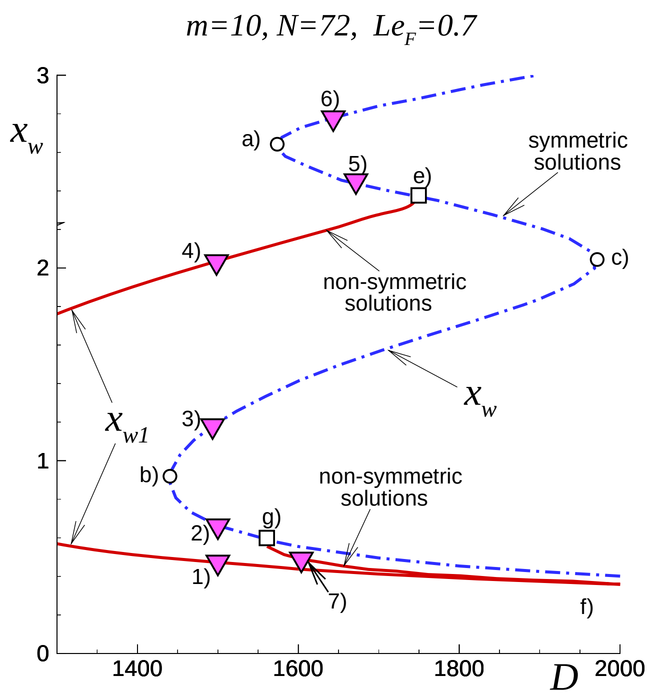


Figure 6: Enlarged fragment of Fig. 5 illustrating the multiplicity of modes. Filled triangles with numbers indicate the points corresponding to the distributions presented in Figs. 2 and 7.

least the solutions corresponding to points 1), 2) and 5) represent stable solutions: they were found to be attractors. For other solutions, it is dangerous to draw exhaustive conclusions from time dependent calculations. Strictly mathematically, it is possible that there are initial states from which the flame structure evolves to other solutions (the authors did not find them). However, the following observation can be made from Fig.5. It can be seen in this figure that only solutions 1), 2) and 5) lie on the branches, along which with increasing Damköhler number both positions of the flame edge approach the porous plug (for solutions 2) and 5) $x_{w1} = x_{w2}$ are equal in magnitude). Of course, this is not a proven criterion.

The symmetry index $S$ defined by Eq. (13) is plotted in Fig. 8 as a function of the Damköhler number with a solid curve for $m = 10$, $Le_F = 0.7$ and

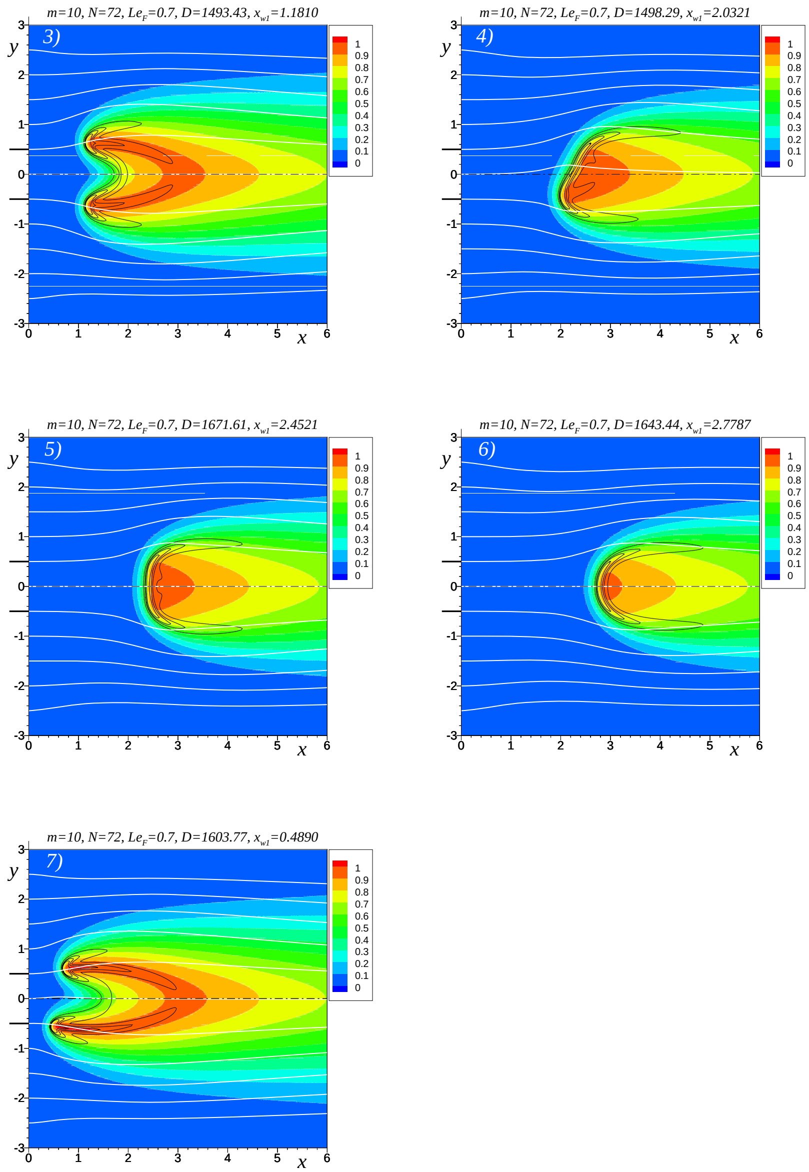


Figure 7: Steady-state solutions corresponding to filled triangles 3), 4), 5), 6) and 7) in Fig. 6. The color shades show the temperature field, black and white lines show $\omega$-isolines ($\omega = 1$, 5, 10 and 20) and $\psi$-isolines (with an interval of 5), respectively.

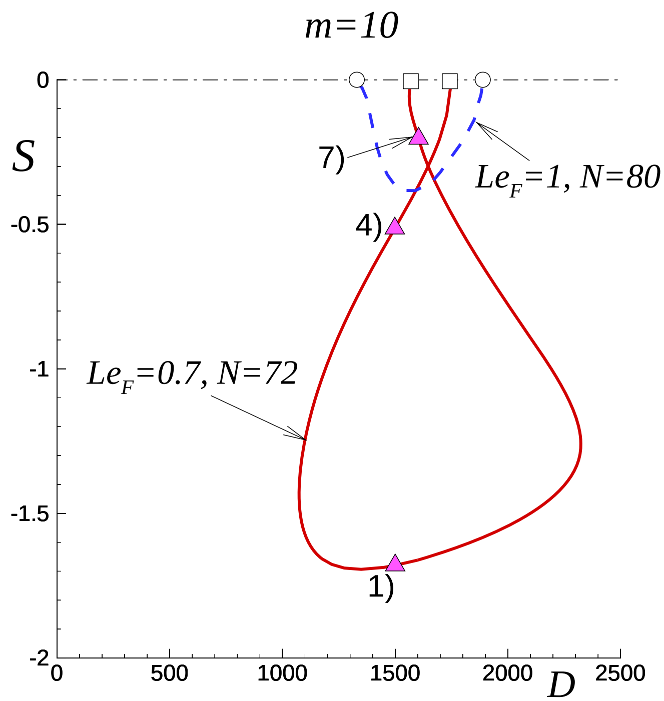


Figure 8: Dependence of the symmetry index $S$ on $D$ calculated for $m = 10$; a solid curve - $L_F = 0.7$ and $N = 72$, a dashed line - $Le_F = 1$ and $N = 80$. The open triangles indicate the points corresponding to plots in Figs. 2 and 7.

$N = 72$. Open squares mark the bifurcation points. The filled triangles 1), 4) and 7) indicate the values corresponding to the non-symmetrical solutions presented in Figs. 2 and 7.

Calculations were also carried out for other values of the flow rate. Fig 9 shows the dependence of the edge flame position calculated for $m = 8$ (left plot) and $m = 6.5$ (right plot) on the Damköhler number for $Le_F = 0.7$ and $N = 72$. Observe that for $m = 8$ the behavior of the dash-dotted curve (symmetric solutions) is qualitatively similar to that for $m = 10$ in Fig. 5. However, for $m = 6.5$, the turning points b) and c) disappear and the double C-shape of the symmetrical branch disappears also. This is the result of a fold-type singularity for decreasing flow rate in the variables $D$, $m$, and $x_w$ for the symmetric solution branch. This means in all likelihood that for

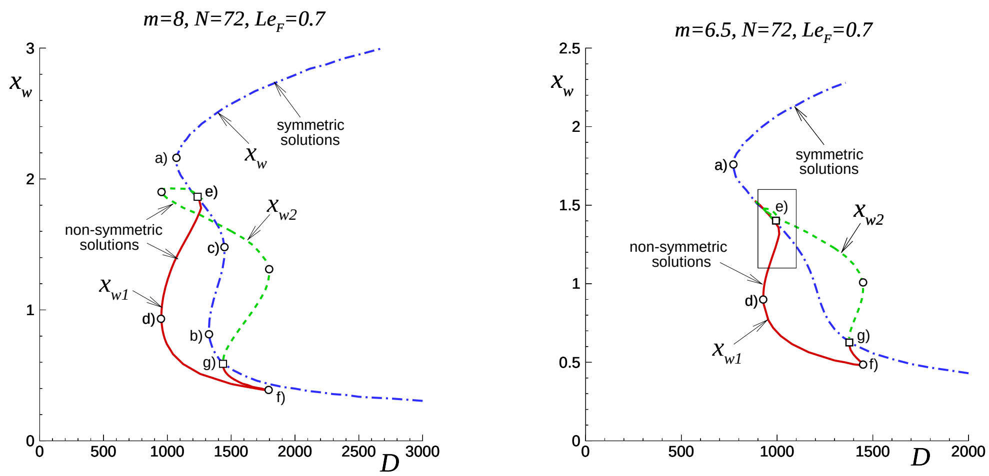


Figure 9: Dependencies of $x_{w1}$, $x_{w2}$ and $x_w$ on $D$ for $N = 72$ and $Le_F = 0.7$; the left plot - $m = 8$, the right plot - $m = 6.5$. The solid and dashed lines show $x_{w1}$ and $x_{w2}$ for non-symmetrical flames, the dash-dotted line shows $x_w$ for symmetrical flames. Open squares indicate bifurcation points; open circles mark the turning points.

low flow rates there are no stable symmetrical solutions located far from the porous plug, similar to the solution 5) shown in Fig. 7 for $m = 10$. It can be seen also that the range of existence of non-symmetric solutions decreases with a decreasing flow rate. This is in agreement with the results reported in [1] obtained within the constant density model.

Fig. 10 shows the behavior of the position of the edge flame near the bifurcation point, where the non-symmetric solution bifurcates from the symmetric one. This zone is marked by a rectangle in Fig. 9. It is interesting that the behavior of $x_{w2}$ has a complex character when the position of the second flame edge (dashed curve) makes a loop.

All the results presented so far have been obtained for $Le_F = 0.7$. It was interesting, however, to find that for $Le_F = 1$ there is a range of parameters where non-symmetric steady-state edge flames configurations exist[3], even if in the present case it is a rather small range. Figure 11 shows the depen-

[3]The possibility of the existence of non-symmetrical configurations for $Le_F = 1$ may have been missed in [1]. However, the difference in the formulations in [1] and in the present study may be the reason why no symmetric solutions were found in [1].

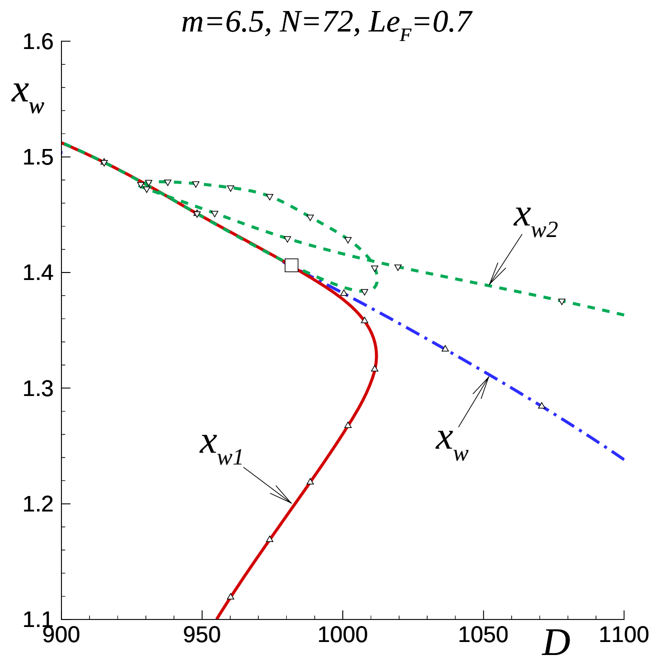


Figure 10: The behavior of the edge flame position inside the square shown in Fig. 9 (right plot) in the vicinity of the bifurcation point (open square). The curve for $x_{w2}$ makes a loop near the bifurcation point. Small triangles show calculated points.

dencies of the edge-flame position on the Damköhler number for symmetric (dashed-dotted line) and non-symmetric (solid and dashed lines) configurations calculated for $Le_F = 1$, $m = 10$ and $N = 80$. The dependence of the symmetry index $S$ on the Damköhler number is shown in Fig. 8 for $Le_F = 1$ with a dashed line. We also note that the dimensionless activation energy is chosen a little higher to obtain non-symmetric solutions with $Le_F = 1$ than it was for $Le_F = 0.7$. An example of the non-symmetrical configuration calculated for $Le_F = 1$ and $D = 1800$ is illustrated in Fig. 12. It can be seen that although the degree of asymmetry is small, the flame configuration is clearly not symmetrical.

The number of solutions is determined by turning and bifurcation points. Figure 13 shows a map of the solution number in the $m - D$ plane for $Le_F =$

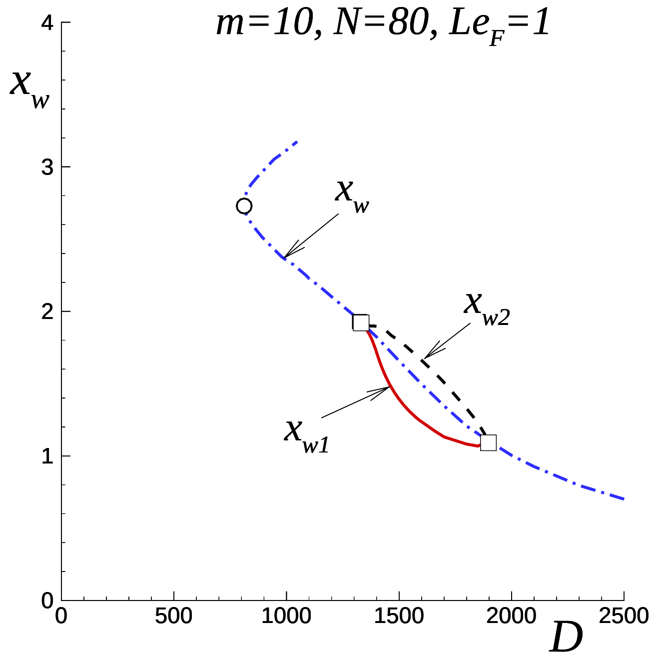


Figure 11: The dependence of the positions of the edge flames on the Damköhler number for $m = 10$, $N = 80$ and $Le_F = 1$. Non-symmetrical flame: $x_{w1}$ - solid line, $x_{w2}$ - dashed line; symmetrical flame: $x_w$ - dash-dotted line. An open circle indicates the turning point for the branch of symmetric solutions and open square symbols mark the bifurcation points for the non-symmetric branch.

0.7. The letters identifying the lines correspond to the points marked with the same letters in Figs. 5 and 9. The numbers inside each zone indicate the number of steady-state solutions. It can be seen that with a gradual increase in the Damköhler number (for fixed $m$), symmetric solutions appear at $m \lesssim 7.24$, and non-symmetric solutions appear at $m \gtrsim 7.24$. This value is determined by the intersection point of the lower dashed-dotted curve and the lower dashed curve. Curves d) and e) merge at $m \approx 6.43$, that is, for smaller values of $m$, there are only two non-symmetric solutions for values of $D$ between the dashed and dash-dotted lines for $m \lesssim 6.43$.

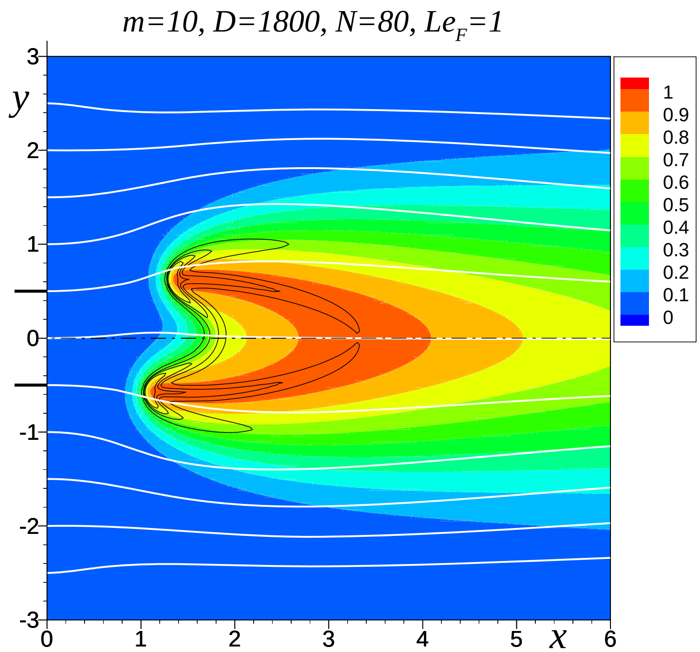


Figure 12: An example of a steady-state non-symmetrical configuration calculated for $m = 10$, $D = 1800$, $N = 80$ and $Le_F = 1$. The color shades show the temperature field, black and white lines show $\omega$-isolines ($\omega = 1$, 5, 10 and 20) and $\psi$-isolines (with an interval of 5), respectively.

### *4.2. Time-dependent calculations*

Time-dependent simulations are more expensive in computational time than iterative calculations of steady-state solutions. As mentioned above, the authors assume that those solutions which belong to the segments of the response curves for which $x_{w1}$ and $x_{w2}$ decrease as $D$ increases are stable. However, this has been verified only for selected parameter values and is not a substitute for the rigorous linear stability analysis remaining outside the scope of the present work.

As was observed in [1] within the constant density model, the setting of one or another steady-state regime depends on the initial conditions. The results obtained in the current work within the variable density model are

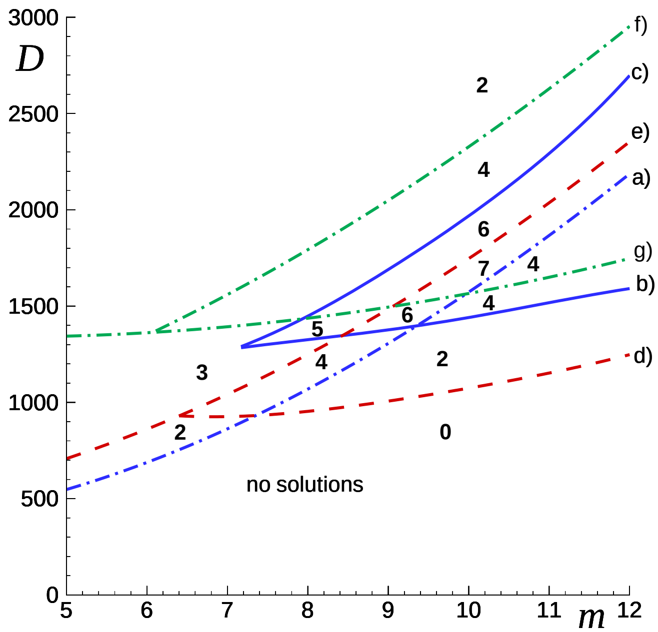


Figure 13: Map of the multiplicity of steady-state modes in the $m - D$ parameters plane, calculated for $Le_F = 0.7$ and $N = 72$. Letters correspond to turning points and bifurcation points in Figs. 5 and 9. The numbers indicate the number of non-trivial solutions in each area. The given number of solutions does not take into account the non-symmetric partner solutions mirrored with respect to the axis of symmetry. There are no non-trivial solutions for the values of $D$ under the dash-dotted and lower dashed curves.

presented in Figs. 14, 15 and 16. These figures show selected snapshots of temperature distributions (colored shades) and isolines of the reaction rate (black lines). All calculations were carried out for $m = 10$, $D = 1685$, $Le_F = 0.7$, $N = 72$ and $Pr = 0.72$. Note that the time-dependent cases were calculated for a small but non-zero value of the Mach number.

For the example shown in Fig. 14, the initial temperature distribution was chosen as a single hot spot located below the symmetry line and relatively close to the porous plug, $x_* = 1$ and $y_* = -0.5$. The sequence of snapshots demonstrates that after a transition period, a non-symmetrical flame state is established, similar to that of Fig. 2 (right plot). Figure 15 demonstrates

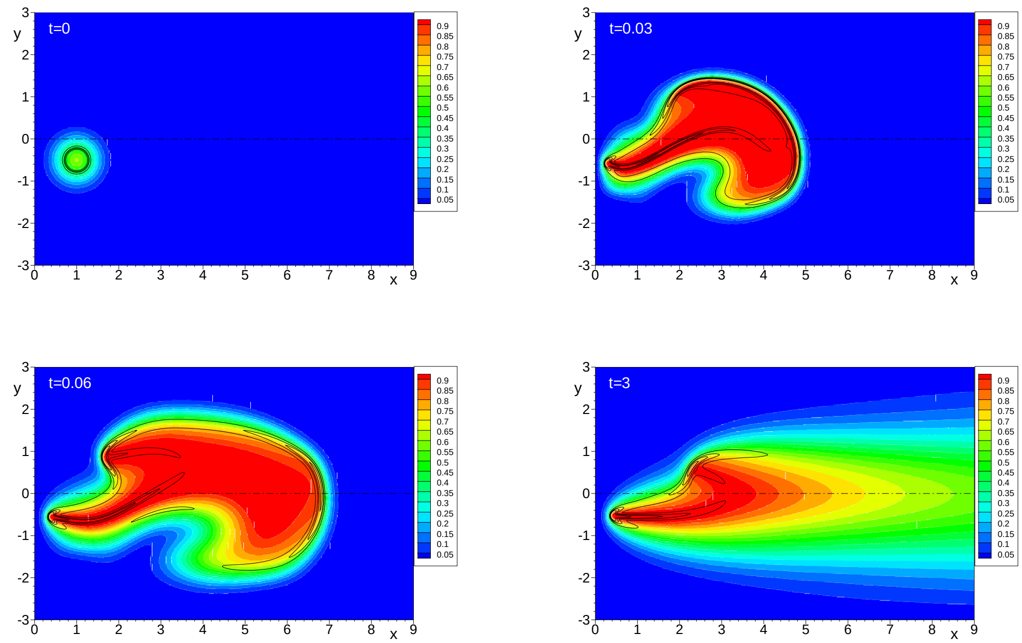


Figure 14: An example of snapshots of the flame dynamics initiated after a single hot spot situated at $x_* = 1$ and $y_* = -0.5$ corresponding to $t = 0$, $t = 0.03$, $t = 0.06$, $t = 3$. The flame structure at long times is similar to solution 1) in Fig. 2.

that if the hot spot is located closer to the symmetry line than in the previous case, namely with $x_* = 1$ and $y_* = -0.2$, then the final structure after long times is a symmetrical state with two symmetrically located edge flames. A similar trend was also described in [1] where the constant density model was applied. It was found that there was a critical value for the vertical position of the hot spot, which determined whether symmetric or non-symmetric solutions were obtained, while other parameters were fixed. And finally, Fig. 16 demonstrates that when the initial temperature distribution is chosen as a single hot spot located on the axis of symmetry and sufficiently distant from the porous plug, $x_* = 4$ and $y_* = 0$, then after a transitional period of time a flame state similar to state e) shown in Fig. 7 is approached.

Table 1 compares the values of the edge flame position closest to the porous plug, $x_{w1}$ obtained using iterative and time-dependent calculation methods. It can be seen that these quantities coincide with satisfactory

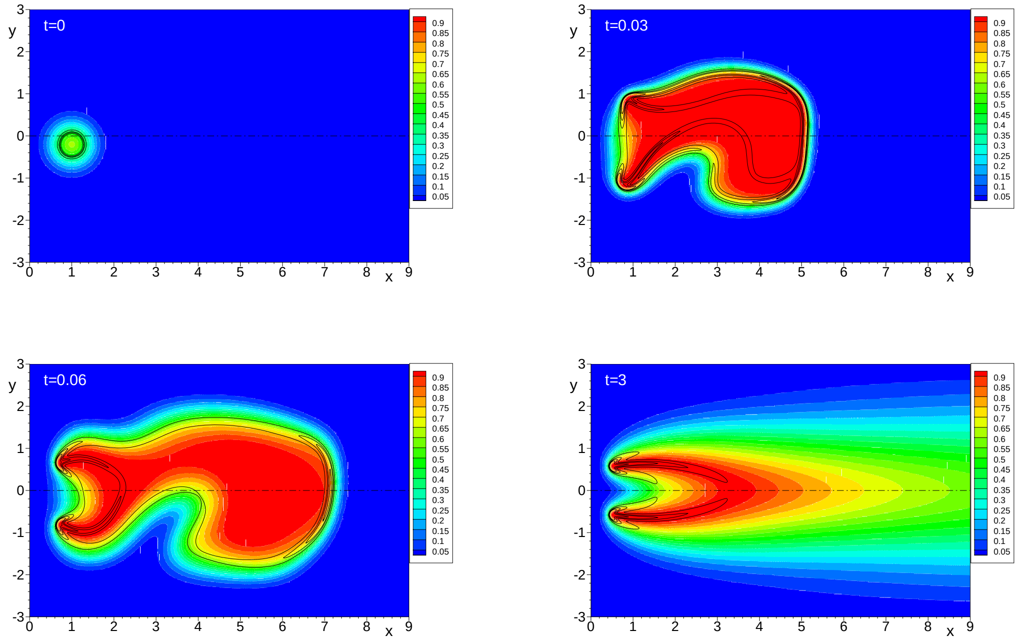


Figure 15: An example of snapshots of the flame structures initiated after a hot spots situated at $x_* = 1$ and $y_* = -0.2$ corresponding to $t = 0$, $t = 0.03$, $t = 0.06$, $t = 3$. The flame structure at long times is similar to solution 2) in Fig. 2.

accuracy for the asymmetric solution 1) and the symmetric nearest to the porous plug solution 2). For a remote symmetric solution 5), the match is worse, which can be attributed to the following reason. It should be noted that when using the time-dependent code, relatively small flame oscillations caused by the flame-acoustic interaction were observed. As is well known, this effect depends on the geometry (channel length) and the boundary conditions used at its outlet. Nevertheless, the numerical differences for $x_{w1}$ for the remote solution obtained from different codes are not significant being purely quantitative in nature and the distributions are almost identical in their structure. Time dependent calculations have shown that solutions of this type are stable (this solution is an attractor for some type of initial conditions) if the effect of possible flame-acoustic interactions is omitted. The role of acoustic instabilities will be explored elsewhere.

The types of flame dynamics in all the cases shown are similar to each

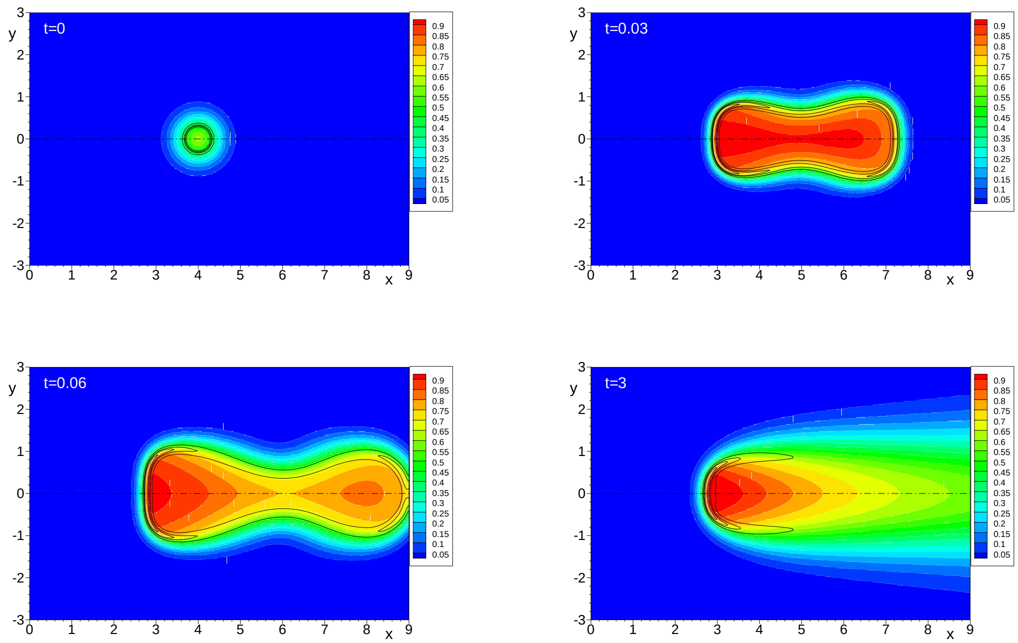


Figure 16: An example of snapshots of the flame structures initiated after a single hot spot situated at $x_* = 4$, $y_* = 0$ corresponding to $t = 0$, $t = 0.03$, $t = 0.06$, $t = 3$. The flame structure at long times is similar to solution 5) in Fig. 7.

other in some sense. As the hot spots are applied to the cold distribution of the fuel and oxidizer, where the mixing zones have already been formed, two combustion waves propagate from the heated region upstream and downstream. After a certain period of time, the downstream moving wave leaves the numerical domain and the steady-state distributions of the variables are established. These are only examples and do not intend to determine the area of attraction of one regime or another. With all probability, one can expect that the three stable states described above can be obtained from other initial conditions.

## 5. Conclusions

The phenomenon of multiplicity of combustion regimes is often encountered in combustion problems. An example is freely propagating premixed

| | solution 1) | solution 2) | solution 5) |
|---|---|---|---|
| steady code | 0.429 | 0.491 | 2.55 |
| time-dependent code | 0.428 | 0.493 | 2.65 |

Table 1: Comparison of the flame edge positions for the edge closest to the porous plug obtained using iterative and time-dependent methods, for $D = 1683$, $m = 10$, $Le_F = 0.7$ and $N = 72$.

flames in narrow channels with heat losses. In this case two solutions exist usually, one is stable and the other is unstable. The multiplicity is observed for the phenomenon of symmetry breaking for premixed flames propagating in adiabatic channels, when two states of the flame, symmetric and non-symmetric, exist simultaneously for some values of the parameters. In this case, the non-symmetric state (when it exists) is usually stable, and the symmetric state is not. However the situations with multiple regimes, when there are several stable steady states, have received little attention. For diffusion flames, according to the best knowledge of the authors, the problem of symmetry breaking was addressed only in [1], within the framework of the constant density model. The present study is trying to fill this gap, and revisit this problem on the basis of the Navier-Stokes equations combined with the equations of transport of species and energy.

The problem of the two edge flames formed when a planar stream of fuel is surrounded on both sides by streams of oxidizer is formulated here in such a way that the governing equations and boundary conditions are symmetrical with respect to the axis of symmetry of the problem. The analysis shows that at least seven different steady-state solutions can exist simultaneously for some values of the parameters, and at least three of them are non-symmetrical. However, if we take into account that every non-symmetric solution has a mirror partner, then the total number of solutions can be at least up to ten. We should remark that this research is not exhaustive and does not cover all the parametric range of possible solutions. We want to emphasize that other, different solutions, might exist in another parametric region.

The results presented seem to be important from several points of view. Firstly, if numerical simulations are performed in half the domain to reduce computational costs, then there is a possibility that the parametrical range of flame existence will be determined incorrectly. Indeed, the possibility of symmetry breaking effect in this case is eliminated a priori. Secondly, the simultaneous existence of symmetric and non-symmetric solutions and the different interaction of the flames with the device in the two cases can lead to difficulties in the device operation.

It is possible to generalize the formulation. Let us assume that the degree of symmetry in the problem formulation depends on one (for the sake of simplicity) parameter, for example, say $\alpha$. It could be a position of the centerline of the fuel stream relative to the axis of the channel, for example. Thus, for $\alpha = 0$, the equations and boundary conditions are symmetric and, as shown, and there are up to seven (ten) non-trivial different solutions, of which at least three are apparently stable.

When $\alpha$ deviates from zero, the symmetry of the problem is broken. However, it is clear that for not very large deviations of $\alpha$ from zero, the total number of solutions must be preserved, due to the continuous dependence of solutions on the parameter. Of course, the classification of solutions into symmetric and non-symmetric loses its meaning.

**Acknowledgment**

This study was supported by MCIN with funding from European Union NextGenerationEU (PRTR-C17.I1) as well by grants #PID2019-108592RBC 42AEI/ 10.13039/501100011033/ and #TED2021-129446-C42/ AEI/10.130 39/501100011033/NextGenerationEU /PRTR.

## References

[1] V.N. Kurdyumov, C. Jiménez, Lifted jet edge flames: symmetric and non-symmetric configurations, *Combust. Theor. Model.* 26 (2022) 1114-1129.

[2] N. Peters, Local quenching due to flame stretch and non-premixed turbulent combustion, *Combust. Sci. Tech.* 30 (1983) 1-17.

[3] J. Buckmaster, M. Matalon, Anomalous Lewis number effect in tribranchial flames, *Symp. (Int.) Combust.* 22 (1988) 1527-1535.

[4] G.R. Ruetsch, L. Vervisch, A. Liñán, Effects of heat release on triple flames, *Phys. Fluids A* 7 (1995) 1447-1454.

[5] J. Buckmaster, Edge-flames and their stability, *Combust. Sci. Tech.* 115 (1996) 41-68.

[6] J. Daou, A. Liñán, The role of unequal diffusivities in ignition and extinction fronts in strained mixing layers, *Combust. Theor. Model.* 2 (1998) 449477.

[7] S. Ghosal, L. Vervisch, Theoretical and numerical study of a symmetrical triple flame using the parabolic flame path approximation, *J. Fluid Mech.* 415 (2000) 227-260.

[8] V. Nayagam, F. Willams, Lewis-number effects in edge-flame prapagation, *J. Fluid Mech.* 458 (2002) 219-228.

[9] R. Daou, J. Daou, J. Dold, Effect of heat-loss on flame-edges in a premixed counterflow, *Combust. Theor. Model.* 7 (2003) 221242.

[10] R.W. Thatcher, A.A. Omon-Arancibia, Multiple speeds of flame edge propagation for Lewis numbers above one, *Combust. Theor. Model.* 9 (2005) 647-658.

[11] M.S. Cha, P.D. Ronney, Propagation rates of nonpremixed edge flames, *Combust. Flame* 146 (2006) 312-328.

[12] J. Daou, F. Al-Malki, Triple-flame propagation in a parallel flow: an analytical study, *Combust. Theor. Model.* 14 (2010) 177202.

[13] P. Pearce, J. Daou, The effect of gravity and thermal expansion on the propagation of a triple flame in a horizontal channel, *Combust. Flame* 160 (2013) 2800-2809.

[14] V.N. Kurdyumov, M. Matalon, Radiation losses as a driving mechanism for flame oscillations, *Proc. Combust. Inst.* 29 (2002) 45-52.

[15] V.N. Kurdyumov, M. Matalon, Dynamics of an edge flame in a mixing layer, *Combust. Flame* 139 (2004) 329-339.

[16] V.N. Kurdyumov, M. Matalon, Stabilization and onset of oscillation of an edge-flame in the near-wake of a fuel injector, *Proc. Combust. Inst.* 31 (2007) 909-917.

[17] V. Kurdyumov, M. Matalon, Effects of thermal expansion on the stabilization of an edge-flame in a mixing-layer model, *Proc. Combust. Inst.* 32 (2009) 1107-1115.

[18] J.A. Bieri, M. Matalon, Edge flames stabilized in a non-premixed microcombustor, *Combust. Theor. Model.* 15 (2011) 911-932.

[19] J.A. Bieri, V.N. Kurdyumov, M. Matalon, The effect of gas expansion on edge flames stabilized in narrow channels, *Proc. Combust. Int.* 33 (2011) 1227-1234.

[20] K.-P. Liao, M. Matalon, C. Pantano, A flow pattern that sustains an edge flame in a straining mixing layer with finite thermal expansion, *Proc. Combust. Inst.* 35 (2015) 1015-1021.

[21] Z. Lu, M. Matalon, Edge flames in mixing layers: Effects of heat recirculation through thermally active splitter plates, *Combust. Flame* 217 (2020) 262-273

[22] B. Shields, J.B. Freund, C. Pantano, Stationary edge flames in a wedge with hydrodynamic variable-density interaction, *Combust. Flame* 211 (2020) 347-361.

[23] V.N. Kurdyumov, M. Matalon, Dynamics of an edge-flame in the corner region of two mutually perpendicular streams, *Proc. Combust. Inst.* 31 (2007) 929-938.

[24] J.Buckmaster, Edge-flames, *Prog. Eng. Combust.* 28 (2002) 435-475.

[25] S.H. Chung, Stabilization, propagation and instability of tribrachial triple flames, *Proc. Combust. Inst.* 31 (2007) 877-892.

[26] K.M. Lyons, Toward an understanding of the stabilization mechanisms of lifted turbulent jet flames: Experiments, *Prog. Energ. Combust.* 33 (2007) 211-231.

[27] A. Liñán, M. Vera, A.L. Sanchez, Ignition, liftoff, and extinction of gaseous diffusion flames, *Annu. Rev. Fluid Mech.* 47 (2015) 293-314.

[28] J. Carpio, Ph. D thesis, UPM 2008.

[29] V. N. Kurdyumov, E. Fernández-Tarrazo, Lewis number effect on the propagation of premixed laminar flames in narrow open ducts, *Combust. Flame* 128 (2002) 382–394.

[30] C. H. Tsai, The asymmetric behavior of steady laminar flame propagation in ducts, *Combust. Sci. Tech.* 180 (2008) 533–545.

[31] V.N. Kurdyumov, Lewis number effect on the propagation of premixed flames in narrow adiabatic channels: Symmetric and non-symmetric flames and their linear stability analysis, *Combust. Flame* 158 (2011) 1307–1317.

[32] V.N. Kurdyumov, C, Jiménez, Structure and stability of premixed flames propagating in narrow channels of circular cross-section: Non-axisymmetric, pulsating and rotating flames, *Combust. Flame* 167 (2016) 149–163.

[33] C. Jiménez, V.N. Kurdyumov, Propagation of symmetric and non-symmetric lean hydrogen-air flames in narrow channels: Influence of heat losses, *Proc. Combust. Inst.* 36 (2017) 1559-1567.

[34] A. Dejoan, V.N. Kurdyumov, Thermal expansion effect on the propagation of premixed flames in narrow channels of circular cross-section: Multiplicity of solutions, axisymmetry and non-axisymmetry, *Proc. Combust. Inst.* 37 (2019) 1927-1935.

[35] T. Poinsot and D. Veynante, S. Candel, Quenching processes and premixed turbulent combustion diagrams, *J. Fluid Mech.*, 228 (1991) 561-606.

[36] Williams, F. A., Combustion Theory, 2nd ed., The Benjamin/Cummings Publishing Company, 1985.

# Table caption

**Table 1.** Comparison of the flame edge positions for the edge closest to the porous plug obtained using iterative and time-dependent methods, for $D = 1683$, $m = 10$, $Le_F = 0.7$ and $N = 72$.

# Figure captions

**Figure 1.** Sketch of the problem, coordinate system, distributions of the normalized mass fraction of fuel (solid isolines, with an interval of 0.1) and the stream function (dashed isolines, with an interval of 5) plotted for $m = 10$ and the frozen case, $D = 0$
**Figure 2.** Example of two flame structures, non-symmetrical (left plot) and symmetrical (right plot) calculated with the same set of parameters, $m = 10$, $D = 1500$, $N = 72$ and $Le_F = 0.7$. The solutions correspond to points 1) and 2) in Fig. 6; the color shades show the temperature field, black and white lines show $\omega$-isolines ($\omega = 1$, 5, 10 and 20) and $\psi$-isolines (with an interval of 5), respectively.
**Figure 3.** Dependence of the heat flux $q$ on $y$ along the porous plug for symmetrical and non-symmetrical configurations, for $m = 10$, $D = 1500$, $N = 72$ and $Le_F = 0.7$.
**Figure 4.** The symmetry index $S$ (solid line) and the position of the leading edge flame for the symmetrical (dashed line) and non-symmetrical (dash-dotted line) cases versus the Zel'dovich number, for $m = 10$, $D = 1500$ and $Le_F = 0.7$.
**Figure 5.** Dependence of the edge flame position on the Damköhler number for $m = 10$, $N = 72$ and $Le_F = 0.7$. The solid and dashed lines show $x_{w1}$ and $x_{w2}$, respectively, for non-symmetrical flames, the dash-dotted line represents $x_w$ for symmetrical flames; open circles mark the turning points; open squares indicate the bifurcation points.
**Figure 6.** Enlarged fragment of Fig. 5 illustrating the multiplicity of modes. Filled triangles with numbers indicate the points corresponding to the distributions presented in Figs. 2 and 7.
**Figure 7.** Steady-state solutions corresponding to filled triangles 3), 4), 5), 6) and 7) in Fig. 6. The color shades show the temperature field, black and white lines show $\omega$-isolines ($\omega = 1$, 5, 10 and 20) and $\psi$-isolines (with an interval of 5), respectively.
**Figure 8.** Dependence of the symmetry index $S$ on $D$ calculated for $m = 10$;

a solid curve - $L_F = 0.7$ and $N = 72$, a dashed line - $Le_F = 1$ and $N = 80$. The open triangles indicate the points corresponding to plots in Figs. 2 and 7.

**Figure 9.** Dependencies of $x_{w1}$, $x_{w2}$ and $x_w$ on $D$ for $N = 72$ and $Le_F = 0.7$; the left plot - $m = 8$, the right plot - $m = 6.5$. The solid and dashed lines show $x_{w1}$ and $x_{w2}$ for non-symmetrical flames, the dash-dotted line shows $x_w$ for symmetrical flames. Open squares indicate bifurcation points; open circles mark the turning points.

**Figure 10.** The behavior of the edge flame position inside the square shown in Fig. 9 (right plot) in the vicinity of the bifurcation point (open square). The curve for $x_{w2}$ makes a loop near the bifurcation point. Small triangles show calculated points.

**Figure 11.** The dependence of the positions of the edge flames on the Damköhler number for $m = 10$, $N = 80$ and $Le_F = 1$. Non-symmetrical flame: $x_{w1}$ - solid line, $x_{w2}$ - dashed line; symmetrical flame: $x_w$ - dash-dotted line. An open circle indicates the turning point for the branch of symmetric solutions and open square symbols mark the bifurcation points for the non-symmetric branch.

**Figure 12.** An example of a steady-state non-symmetrical configuration calculated for $m = 10$, $D = 1800$, $N = 80$ and $Le_F = 1$. The color shades show the temperature field, black and white lines show $\omega$-isolines ($\omega = 1$, 5, 10 and 20) and $\psi$-isolines (with an interval of 5), respectively.

**Figure 13.** Map of the multiplicity of steady-state modes in the $m - D$ parameters plane, calculated for $Le_F = 0.7$ and $N = 72$. Letters correspond to turning points and bifurcation points in Figs. 5 and 9. The numbers indicate the number of non-trivial solutions in each area. The given number of solutions does not take into account the non-symmetric partner solutions mirrored with respect to the axis of symmetry. There are no non-trivial solutions for the values of $D$ under the dash-dotted and lower dashed curves.

**Figure 14.** An example of snapshots of the flame dynamics initiated after a single hot spot situated at $x_* = 1$ and $y_* = -0.5$ corresponding to $t = 0$, $t = 0.03$, $t = 0.06$, $t = 3$. The flame structure at long times is similar to solution 1) in Fig. 2.

**Figure 15.** An example of snapshots of the flame structures initiated after a hot spots situated at $x_* = 1$ and $y_* = -0.2$ corresponding to $t = 0$, $t = 0.03$, $t = 0.06$, $t = 3$. The flame structure at long times is similar to solution 2) in Fig. 2.

**Figure 16.** An example of snapshots of the flame structures initiated after

a single hot spot situated at $x_* = 4$, $y_* = 0$ corresponding to $t = 0$, $t = 0.03$, $t = 0.06$, $t = 3$. The flame structure at long times is similar to solution 5) in Fig. 7.